ISBN 978-989-9121-55-3
64th ISTANBUL World Congress on Innovations in "Science, Engineering, Technology & Education" (WCISET-25)
Nov. 13-14, 2025 Istanbul (Türkiye)

Optimizing Magnetometers and Systems Modeled by the Bloch Equation Through Parametric Resonance

Asma Benbouza[1] and M.S.B Bouza[2]
[1]Department of Physics, University of Science and Technology of China, Hefei, 230026, People's Republic of China
[2]Department of Physics, University of Science and Technology of Batna 1, Batna, 05000, Algeria

Abstract: *Precise detection of weak magnetic fields is fundamental to applications ranging from biomedical imaging to quantum sensing. This work presents an approach to optimize the performance of radiofrequency (RF) magnetometers through parametric resonance tuning, guided by the Bloch equations describing spin-field interactions. In realistic conditions, spin relaxation due to collisions and spin exchange leads to signal decay and broadened resonance peaks. To counter this, a small periodic modulation is applied to the magnetic field, effectively modulating the Larmor frequency. When the modulation satisfies the resonance condition, energy is periodically transferred back to the spin ensemble, sustaining polarization and narrowing the resonance linewidth. The results demonstrate that controlled parametric driving can substantially improve the stability and sensitivity of RF magnetometers, offering a strong framework for precision magnetic field sensing in complex and fluctuating environments.*

Keywords*: Bloch Equations, Parametric Resonance, Spin Relaxation, RF Magnetometers, Larmor Frequency, Quantum Sensing, Hybrid Quantum Devices, MRI*

1. Introduction

Atomic magnetometers have emerged as exceptionally sensitive instruments for detecting weak magnetic fields, bridging fundamental research and applied technologies across physics, medicine, and engineering [1–4]. Their operation relies on detecting magnetic resonance in atomic ensembles, where the collective spin dynamics of alkali or noble gas atoms provide a precise probe of magnetic field variations [5, 6]. Advances in optical pumping, spin-exchange relaxation suppression, and field modulation techniques have pushed sensitivities to the sub-femtotesla regime, even under unshielded conditions [2, 7, 8]. These features make atomic magnetometers valuable not only for geomagnetic exploration and quantum control but also for biomedical imaging, where they serve as non-invasive alternatives to cryogenic SQUID systems in detecting neuronal or cardiac magnetic activity [9]. While in physics, they provide tools for probing spin-exchange dynamics, testing fundamental symmetries, and exploring light–matter interactions in the quantum regime [6, 10]. Their high sensitivity, room temperature operation, and tunable frequency response establish them as compact, field-deployable tools for precision measurements in fluctuating environments [10]. Among the diverse magnetometric techniques, parametric resonance magnetometers (PRMs) have gained renewed attention for their ability to achieve high sensitivity through resonance amplification under time varying driving fields [11, 12]. In these systems, the spin precession is not only determined by the static magnetic field but also by the modulation parameters of the radiofrequency (RF), which introduce a periodic variation in the effective potential [13, 14]. This interplay between the driving frequency and the intrinsic Larmor frequency gives rise to parametric resonances, analogous to those observed in classical oscillators [13].

Our study builds on this perspective by analyzing the spin dynamics in the rotating reference frame, where the modulation frequency and resonance conditions, play a central role in defining the system's response. By numerically exploring the equations of motion of the driving field, we uncover patterns corresponding to distinct magnetometric sensitivities. These findings are particularly relevant in the context of next generation magnetometry, where hybrid approaches integrate classical control theory, machine learning optimization, and multi-sensor arrays to enhance field reconstruction accuracy and spatial resolution [9, 15].

The article is structured around three main sections. (I) The first section, establishes the theoretical foundation of the study. It derives the equations of motion governing spin polarization in the presence of an external radio-frequency magnetic field, formulated through the Bloch equations. This section highlights the interplay between precession, optical pumping, and relaxation processes, emphasizing how these competing mechanisms shape the evolution of spin coherence and signal formation in atomic magnetometers. (II) The second section, extends the theoretical framework by introducing a timeperiodic modulation of the magnetic field and analysing its influence on the spin response. Here, the emergence of parametric resonance is discussed in relation to the Larmor frequency, revealing how specific modulation conditions lead to energy exchange, and resonance amplification. (III) Finally, the conclusion summarizes the principal findings and discusses their implications for improving the performance of RF magnetometers in noisy and low-frequency environments.

2. Spin Dynamics and Bloch Formalism in RF Magnetometers

Understanding the behavior of atomic spins under the influence of magnetic fields is central to the operation of RF magnetometers. The collective dynamics of these spins determine the device's sensitivity and response to weak magnetic fields. To describe these dynamics quantitatively, we employ the Bloch formalism, which model the evolution of spin polarization and the effects of optical pumping, relaxation, and time-dependent driving fields on the magnetometer's performance.

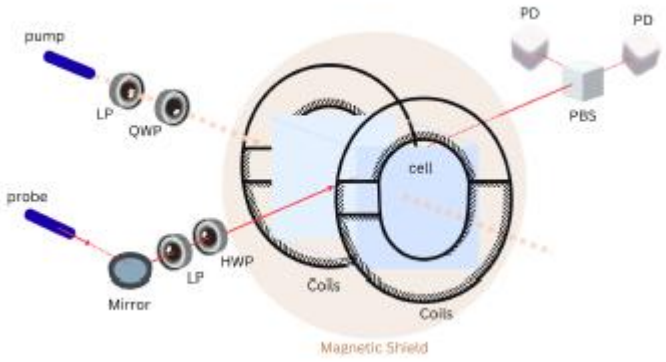

FIG. 1: Schematic of an RF magnetometer operating in a rotating magnetic fieldj

Fig. 1 illustrates the fundamental working principle of spin-based magnetic sensing. In this configuration, an atomic ensemble is exposed simultaneously to a static or slowly varying longitudinal magnetic field and a transverse magnetic field that rotates at a controlled frequency.Optical pumping initializes the atomic spins along a preferred direction, creating a net polarization in the ensemble. As the transverse field rotates, it drives the spins into precession around the effective magnetic field, generating a time-dependent transverse polarization that is detected through optical or electronic readout techniques. The Hamiltonian for a spin particle in a magnetic field is expressed as

$$H = -\gamma S \cdot B, \tag{1}$$

where γ is the gyromagnetic ratio and S is the spin operator. The corresponding Heisenberg equation of motions

$$\frac{d\mathbf{S}}{dt} = \frac{i}{\hbar}[H, \mathbf{S}], \tag{2}$$

leads, in the semiclassical limit, to the equation governing the evolution of the ensemble-averaged spin polarization vector P = ⟨S⟩/N, where N is the number of spins. The resulting Bloch equation takes the form

$$\frac{d\mathbf{P}}{dt} = \gamma\,\mathbf{P} \times \mathbf{B}(t) + R_{\mathrm{OP}}(\mathbf{s} - \mathbf{P}) - \Gamma_0\mathbf{P} \tag{3}$$

where *Rop* denotes the optical pumping rate and Γ0 is the intrinsic relaxation constant. The first term describes the spin precession around the magnetic field **B**(t), while the remaining two represent the competing effects of optical alignment toward the steady-state spin orientation s and damping due to relaxation. The applied magnetic field consists of a rotating transverse component and a modulated longitudinal component

$$\mathbf{B}(t) = B_m \sin(\Omega t)\,\hat{x} + B_m \cos(\Omega t)\,\hat{y} + B_1 \cos(\omega t)\,\hat{z} \tag{4}$$

where Bm and B1 are the amplitudes of the transverse and longitudinal fields, respectively. The angular frequencies *Ω and ω* correspond to the rotation and modulation frequencies of the field.

Eq (3) thus provides a complete description of the polarization dynamics under the combined influence of rf excitation, optical pumping, and relaxation. This framework forms the basis for analyzing resonance phenomena, including the conditions under which the polarization response exhibits parametric amplification near the Larmor frequency. In the absence of Larmor precession (γ = 0), the steady-state solution of Eq. 3 yields

In the absence of Larmor precession (γ = 0), the steady-state solution of Eq. 3 yields

$$P_z = \frac{R_{\mathrm{OP}}}{R_{\mathrm{OP}} + \Gamma_0}\, s, \tag{5}$$

indicating that the longitudinal component approaches an equilibrium value determined by the balance between optical pumping and relaxation. The transverse components decay exponentially with characteristic times T2 = 1/Γ0 and T1 = 1/(ROP + Γ0), as illustrated in Fig. 2.

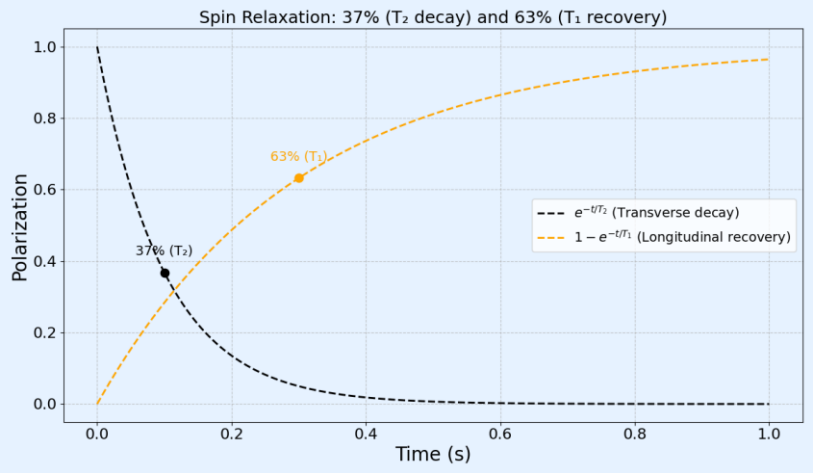

Fig. 2: Transverse and longitudinal decay of spin polarization due to relaxation

The noise floor (NF) of an ideal magnetometer scales inversely with the square root of the detection volume V.

$$\mathrm{NF} \propto V^{-1/2}. \tag{6}$$

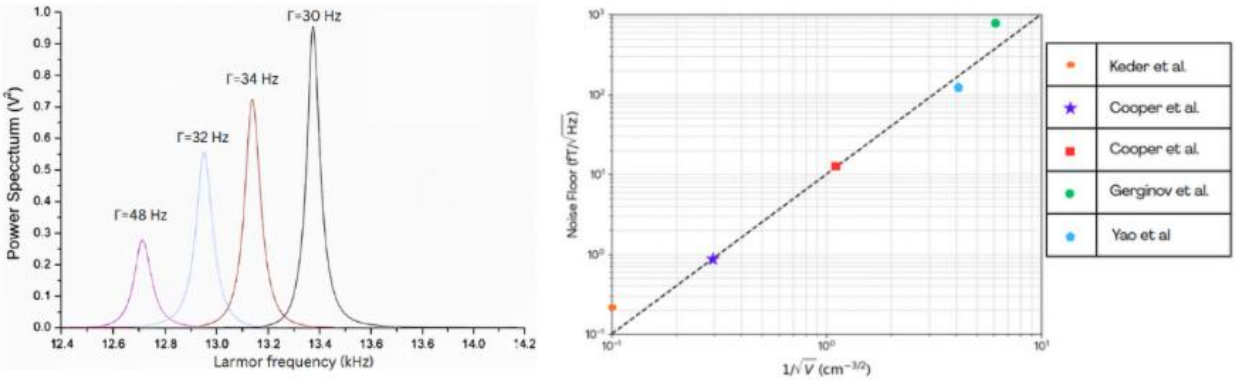

FIG. 3: Spectral profiles and noise spectrum for different relaxation rates [2, 7, 10, 15, 16].

An increase in the relaxation rate Γ broadens the noise peaks in Fig. 3, signaling faster decoherence and reduced spin information retention. Enlarging the cell volume does not necessarily mitigate these losses, as atomic interactions and spin-exchange collisions still contribute to linewidth broadening in Fig. 3. This trade-off highlights the need for active resonance tuning to compensate relaxation losses and recover sharper spectral responses [17, 18].

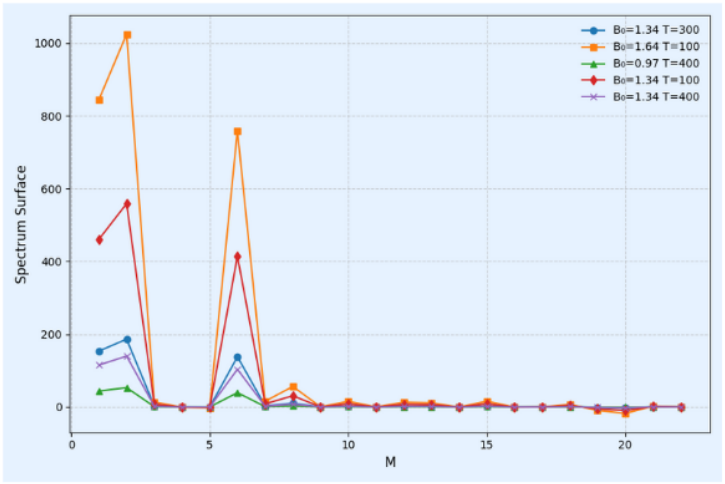

M	Isotope	$\gamma(10^7)$ (rad. s^{-1}. T^{-1})	ν_o (MHz) Freq	$N=N_2/N_1$ -.10-3	$E=h\nu_o$ *1.0e-31	S ($MhzT^3/K$) *1.0e+03	δ(ppm) *1.0e+05
1	^{1}H	26 .75	56.3052	1,0	0.3733	1.4317	-0.985
2	^{3}H	28.53	60.0519	9,65.	0.3981	1.7369	-0.984
3	^{13}C	6,728	14.1615	1,21	0.0939	0.0228	-0.964
4	^{15}N	-2.713	-5.7105	0.159	-0.0379	-0.0015	-1.014
5	^{17}O	-3.628	-7.6365	1.01	-0.0506	-0.0036	-1.0191
6	^{19}F	25 .81	54.3266	1,04.	0.3602	1.2860	-0.986
7	^{23}Na	7.07	14.8814	0.291.10-2	0.0987	0.0264	-0.962
8	^{31}P	10.84	22.8168	0.833	0.1513	0.0953	-0.942
9	^{39}K	1.2498	2.6307	0.925	0.0174	0.0001	-0.933
10	^{51}V	7.0453	14.8294	0.663	0.0983	0.0262	-0.962
11	^{53}Cr	-1.512	-31826	1.09	-0.0211	-0.0003	-1.079
12	^{55}Mn	6.608	13.9090	1.02228	0.0922	0.0216	-0.965
13	^{59}Co	6.317	13.2964	1.02129	0.0882	0.0189	-0.966
14	^{61}Ni	-2.394	-5.0391	0.99193	-0.0334	-0.0010	-1.012
15	^{63}Cu	7.0974	14.9391	1.02392	0.0990	0.0267	-0.962
16	^{91}Zr	-2.4959	-5.2535	0.99159	-0.0348	-0.0012	-1.013
17	^{105}Pd	-1.23	-2.5890	0.99585	-0.0172	-0.0001	-1.065
18	^{127}I	5.3817	11.3278	1.001814	0.0751	0.0117	-0.971
19	^{113}Cd	-5.96	-12.5450	0.997991	-0.0832	-0.0158	-1.031
20	^{129}Xe	-7.3997	-15.5754	0.997506	-0.1033	-0.0303	-1.039
21	^{139}La	3.801	8.0006	1.001281	0.0530	0.0041	-0.979
22	^{197}Au	0.4625	0.9735	1.00156	0.0065	0.0000	0.0170

Fig. 4: Spectrum surface plot and representative nuclear parameters

The nuclear dependence of the magnetic response is expressed as

$$N = \frac{N_2}{N_1} = e^{-\Delta E/k_B T}, \quad \Delta E = h\nu_0 = g_N \mu_N B_0,$$

$$S = kN = \frac{\gamma^3 B_0^3}{T}, \quad \delta = \frac{v_i - v_{\text{ref}}}{v_a B_0} \times 10^6,$$

where N_1 and N_2 denote the populations of the lower and higher nuclear spin states, respectively, while ΔE represents the energy difference between these states. The symbol k_B stands for the Boltzmann constant, T is the absolute temperature, h is Planck's constant, v_0 is the resonance frequency, g_N is the nuclear factor, μ_N is the nuclear magneton, and B_0 is the static magnetic field. The relative frequency shift is denoted by δ, with v_i indicating the observed transition frequency, v_{ref} the reference frequency, and v_a a scaling factor related to the Larmor frequency.

The variation of the spectral surface S(M) for different isotopes in Fig. 4 reveals the interplay between nuclear parameters and magnetic response predicted by the Bloch model in Eq. 3. Heavier nuclei with larger γ exhibit stronger coupling to the external field B_0, leading to enhanced sensitivity. However, this enhancement saturates beyond a certain mass range, implying a limit in spin–field coupling strength. When a weak periodic modulation is introduced to B0, the system enters a regime of parametric resonance near the Larmor frequency, where modulation periodically restores the spin energy lost through relaxation. This mechanism sustains transverse polarization and stabilizes the sensitivity profile for isotopes such as ^{39}K and ^{63}Cu.

3. Parametric Resonance in RF Magnetometers

For a spin in an external magnetic field, Eq. 4, the polarization evolves according to Eq. 3 with an optical pumping rate R_{OP} along s = (0, 0, s). In the rotating reference frame, the Bloch equations governing the spin polarization components $\tilde{P} = (\tilde{P}_x, \tilde{P}_y, \tilde{P}_z)^T$ can be written as

$$\frac{d\tilde{\mathbf{P}}}{dt} = \begin{pmatrix} -\Gamma & \omega_{\text{eff}}(t) & -\Omega_m \\ -\omega_{\text{eff}}(t) & -\Gamma & 0 \\ \Omega_m & 0 & -\Gamma \end{pmatrix} \tilde{\mathbf{P}} + R_{\text{OP}} \begin{pmatrix} 0 \\ 0 \\ s \end{pmatrix} \tag{7}$$

where Γ is the transverse relaxation rate, Ωm the modulation frequency, and ωeff (t) = ω_1 cos (ωt) − Ω represents the effective detuning between the driving field and the Larmor precession frequency, with the effective magnetic field given by

$$\tilde{\mathbf{B}} = \left(0, B_m, B_1 \cos(\omega t) - \frac{\Omega}{\gamma}\right) \tag{8}$$

and Γ = Γ0+ROP, ω1 = γB1, Ωm = γBm. Transforming to a rotating reference frame in the (x, y) plane simplifies the dynamics

$$P_z = P_z, \tilde{P}_x + i\tilde{P}_y = e^{i\Omega t}(P_x + iP_y) \tag{9}$$

The resulting equations show that near the resonance condition ω ∼ Ω/n, the transverse polarization can be strongly amplified:

$$\tilde{P}_x \simeq -\frac{\gamma B_m R_{\text{OP}} s\, J_1^2(\gamma B_1/\omega)}{\Gamma^2 + (\omega - \Omega)^2} \tag{10}$$

The time evolution of the spin components in the rotating frame illustrates how the modulation frequency governs the energy flow within the spin system as seen 4 in Fig. 5. When the modulation frequency satisfies the resonance condition, energy is cyclically restored to the transverse components, preventing their decay and enhancing the overall polarization amplitude.

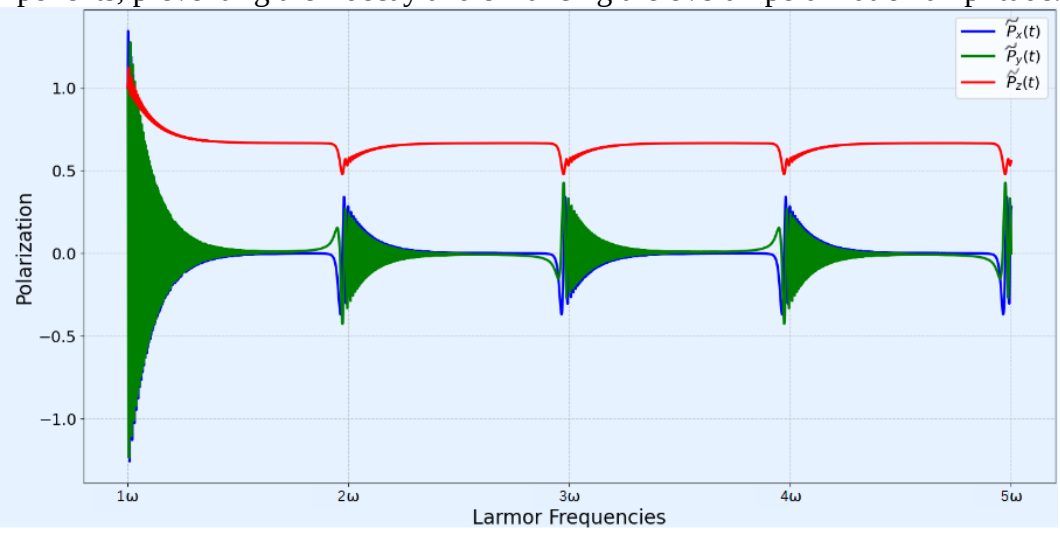

Fig. 5: Parametric resonance of spin polarization in the rotating reference frame.

The analysis reveals that periodic modulation of the magnetic field plays a central role in governing the spin dynamics near resonance. By introducing a controlled time-dependent variation in the field, the system enables a continuous exchange of energy between the external drive and the collective spin ensemble. This modulation effectively sustains the transverse polarization, compensating for relaxation-induced losses and reviving oscillations that would otherwise decay, shown in Fig. 5. When the modulation frequency approaches the Larmor frequency, the system enters the regime of parametric resonance, where the coherent energy transfer amplifies the spin response. This resonant behavior manifests experimentally as a pronounced narrowing of the linewidth and an increase in signal amplitude, reflecting enhanced spin coherence and improved magnetometric sensitivity. Such effects highlight the capacity of parametric driving not only to stabilize polarization but also to unlock new operational regimes for high precision field detection.

These results confirm that parametric driving provides an effective route for improving the performance of RF magnetometers. By maintaining polarization and suppressing elaxation, the method yields sharper resonance features and higher signal-to-noise ratios, which is essential for applications in precision field sensing and low frequency detection environments.

This formulation provides new insight into the mechanisms underlying signal amplification in parametric resonance magnetometry [19]. In particular, the transverse components of the polarization, P_x and P_y, exhibit a pronounced resonant enhancement when the modulation frequency ω approaches the Larmor frequency, revealing the direct coupling between the longitudinal modulation and the spin precession dynamics. The magnitude and sharpness of this resonance are governed by the interplay between the optical pumping rate R_{OP}, the strength of the rotating magnetic field B_m, and the amplitude of the longitudinal modulation B1. Variations in these parameters not only shift the resonance condition but also modify the coherence lifetime of the spin ensemble [20], thus shaping the observed linewidth and signal contrast. Consequently, the derived equations serve as a quantitative framework for interpreting experimentally measured resonance spectra, linking the observed signal features to the underlying spin–field interactions and offering a pathway for optimizing magnetometer performance under realistic operating conditions

4. Conclusion

This work provides a comprehensive analysis of spin dynamics in atomic ensembles under the influence of external radio-frequency magnetic fields, framed through the Bloch formalism. By incorporating a weak periodic modulation into the magnetic field, we demonstrated the emergence of parametric resonance, wherein energy is periodically fed back into the spin ensemble, counteracting relaxation induced losses and sustaining transverse polarization. Our numerical simulations revealed that this mechanism leads to a revival of decaying spin oscillations, sharper resonance features, and enhanced signal amplitude, confirming that modulation near the Larmor frequency effectively stabilizes the spin coherence.

The study also highlights the intricate interplay between key system parameters, including the optical pumping rate, the amplitude of the rotating transverse field, and the longitudinal modulation strength. Variations in these parameters not only influence the resonance condition but also govern the linewidth, signal contrast, and coherence lifetime of the spin ensemble. Additionally, the nuclear dependence of the magnetic response was analyzed, showing that isotopic properties and nuclear spin factors modulate the sensitivity and spectral characteristics of the magnetometer. These insights provide a quantitative framework linking the observed resonance features to the underlying spin–field interactions, offering practical guidelines for optimizing the performance of RF magnetometers under realistic experimental conditions.

Beyond immediate applications in magnetometry, the results underscore the broader relevance of controlled parametric driving for maintaining coherence in dissipative spin systems. The approach has potential implications for precision NMR, hybrid quantum sensors, and quantum information devices, where coherent control over spin ensembles is critical. Future work will aim to experimentally verify these predictions, explore multifrequency modulation schemes, and extend the methodology to complex, multi-spin systems, further advancing the understanding and practical capabilities of high sensitivity magnetic field detection.

5. References

[1] J. C. Allred, R. N. Lyman, T. W. Kornack, and M. V. Romalis, "High-sensitivity atomic magnetometer unaffected by spin-exchange relaxation," Phys. Rev. Lett. 89, 130801 (2002). https://doi.org/10.1103/PhysRevLett.89.130801

[2] David A. Keder, David W. Prescott, Adam W. Conovaloff, and Karen L. Sauer, "An unshielded radio-frequency atomic magnetometer with sub-femtotesla sensitivity," AIP Adv. 4, 127159 (2014). https://doi.org/10.1063/1.4905449

[3] Rachel W. Chan, Justin Y.C. Lau, Wilfred W. Lam, and Angus Z. Lau, "Magnetic resonance imaging," in Encyclopedia of Biomedical Engineering, edited by Roger Narayan (Elsevier, Oxford, 2019) pp. 574–587. https://doi.org/10.1016/B978-0-12-801238-3.99945-8

[4] X. Bai et al., "Atomic magnetometers and their application in industry," Front. in Phys. 11, 1212368 (2023). https://doi.org/10.3389/fphy.2023.1212368

[5] M. P. Ledbetter, I. M. Savukov, V. M. Acosta, D. Budker, and M. V. Romalis, "Spin-exchange-relaxation-free magnetometry with cs vapor," Phys. Rev. A 77, 033408 (2008). https://doi.org/10.1103/PhysRevA.77.033408

[6] Chi Fang, Liwei Jiang, Jiali Liu, Jun Zhu, Qi Shao, Hongyu Pei, and Wei Quan, "Fast measurement of spinexchange relaxation in the range of earth-scale magnetic field," Measurement 221, 113449 (2023). https://doi.org/10.1016/j.measurement.2023.113449

[7] Giuseppe Bevilacqua, Valerio Biancalana, Yordanka Dancheva, and Antonio Vigilante, "Restoring narrow linewidth to a gradient-broadened magnetic resonance by inhomogeneous dressing," Phys. Rev. Appl. 11, 024049 (2019). https://doi.org/10.1103/PhysRevApplied.11.024049

[8] Y. Lu et al., "Recent progress of atomic magnetometers for weak-field applications," Sensors 23, 5318 (2023). https://doi.org/10.3390/s23115318

[9] Yulia Bezsudnova, Andrew J. Quinn, and Ole Jensen, "Optimizing magnetometers arrays and analysis pipelines for multivariate pattern analysis," bioRxiv (2024), 10.1101/2023.09.21.558786. https://doi.org/10.1101/2023.09.21.558786

[10] Robert J. Cooper, David W. Prescott, Karen L. Sauer, Nezih Dural, and Michael V. Romalis, "Intrinsic radiofrequency gradiometer," Phys. Rev. A 106, 053113 (2022). https://doi.org/10.1103/PhysRevA.106.053113

[11] Fran, cois Beato, Elie Belorizky, Etienne Labyt, Matthieu Prado, and Agustin Palacios-Laloy, "Theory of a he 4 parametric-resonance magnetometer based on atomic alignment," Phys. Rev. A 98 (2018), 10.1103/Phys-RevA.98.053431. https://doi.org/10.1103/PhysRevA.98.053431

[12] B. Wang et al., "All-optical parametric-resonance magnetometer based on rf fields," Sensors (2022), 10.3390/s22114184. https://doi.org/10.3390/s22114184

[13] M. Rade, s, "Resonance and antiresonance," in Encyclopedia of Vibration, edited by S. Braun (Elsevier, Oxford, 2001) pp. 1046–1055. https://doi.org/10.1006/rwvb.2001.0163

[14] W. Xiao, X. Liu, Y. Wu, X. Peng, and H. Guo, "Radio-frequency magnetometry based on parametric resonances," App. Phys. Lett. (2024), 10.1103/Phys- RevLett.133.093201. https://doi.org/10.1103/PhysRevLett.133.093201

[15] Han Yao, Benjamin Maddox, and Ferruccio Renzoni, Neural network-aided optimisation of a radiofrequency atomic magnetometer," Opt. Exp. 31, 27287– 27295 (2023). https://doi.org/10.1364/OE.498163

[16] Vladislav Gerginov, Fabio C. S. da Silva, Archita Hati, and Craig Nelson, "An atomic sensor for direct detection of weak microwave signals," IEEE Trans. Microw. Theory Tech. 67, 3485–3493 (2019). https://doi.org/10.1109/TMTT.2019.2921351

[17] M. Padniuk, M. Kopciuch, R. Cipolletti, A. Wickenbrock, D. Budker, and S. Pustelny, "Response of atomic spin-based sensors to magnetic and nonmagnetic perturbations,"Sci Rep (2022), 10.1038/s41598-021-03609-w. https://doi.org/10.1038/s41598-021-03609-w

[18] N. Castagna, G. Bison, G. Di Domenico, A. Hofer, P. Knowles, C. Macchione, H. Saudan, and A. Weis,"A large sample study of spin relaxation and magnetometric sensitivity of paraffin-coated cs vapor cells," App. Phys. B (2009), 10.1007/s00340-009-3464-5. https://doi.org/10.1007/s00340-009-3464-5

[19] H. Zhai, W. Li, and G. Jin, “Improving the sensitivity of a dark-resonance atomic magnetometer,” Sensors 25, 1229 (2025).
https://doi.org/10.3390/s25041229
[20] G. Gao, J. Hu, F. Tang, W. Liu, M. Zhu, and N. Zhao, “Stability improvement of nuclear magnetic resonance gyroscope with self-calibrating parametric magnetometer,”Phys. Rev. App. (2024), 10.1103/PhysRevApplied. 21.014042.
https://doi.org/10.1103/PhysRevApplied.21.014042